RSC Advances

PAPER

View Article Online
View Journal | View Issue

Cite this: *RSC Adv.*, 2019, **9**, 27242

Synthesis of core–shell magnetic titanate nanofibers composite for the efficient removal of Sr(II)†

Rong Yi,*[a] Gang Ye[b] and Jing Chen*[b]

Received 7th August 2019
Accepted 22nd August 2019

DOI: 10.1039/c9ra06148g

rsc.li/rsc-advances

We report a facile approach for the fabrication of Fe_3O_4@titanate fibers magnetic composite through a hydrothermal method and sol–gel process. The structure and morphology were characterized by X-ray diffraction (XRD), transmission electron microsphere (TEM), scanning electron microscope (SEM) and energy-dispersive X-ray analysis (EDX). Owing to the high ion exchange capacity of the functional titanate layer, the obtained core–shell structured magnetic microspheres exhibited high removal efficiency towards strontium from wastewater. The effects of contact time and Sr(II) concentration on the uptake amount of strontium were systematically investigated. The results indicated that the adsorption equilibrium can be reached within 30 min, and the maximum exchange capacity was approximately 37.1 mg g^{-1}. Moreover, the captured Sr(II) can be eluted using 5 wt% of EDTA(Na), which contributed to the reduction of waste volume. Based on the experimental results of ion exchange process and X-ray photoelectron spectroscopy (XPS), a possible adsorption mechanism was proposed. This work provided a facile approach to synthesize magnetic functional nanocomposites for wastewater treatment.

Introduction

Environmental contamination with harmful fission products (FPs), which are generated during the operation of nuclear facilities, has aroused world-wide concern after the nuclear accident at Fukushima, Japan.[1,2] The leak of radionuclides may give rise to a serious threat to human health. For example, ^{90}Sr is one of the typical FPs and is found in operational waste from reactors and reprocessing plants.[3] It was possesses a long half-life ($T_{1/2}$ = 28.5 years), high radioactivity and is a biological hazard. Moreover, ^{90}Sr can substitute for calcium in bones, leading to increased risk of leukemia and other diseases.[4]

In order to address this issue, many techniques have been developed to remove radionuclides from radioactive streams and their subsequent disposal, including membrane distillation,[5,6] reverse osmosis[7,8] and solvent extraction.[9] However, these methods currently deployed to manage radioactive waste can be complex and extremely costly.[10] Inorganic cation exchangers, especially synthetic inorganic cation exchanger materials, such as layered zirconium phosphates synthetic micas,[11,12] titanium molybdophosphate[13] and layered titanate nanofibers,[14–16] are recognized as a promising candidates for the removal of radioactive cations owing to their large ion exchange capacity, high selectivity, excellent irradiation and chemical stability. The radioactive ions can be captured from wastewater through preferentially exchanging with sodium ions or proton in the synthetic materials. Recently, a novel synthetic inorganic exchange, trititanate nanofibers (with a chemical formula $Na_2Ti_3O_7$), has been shown to exhibit high removal efficiency towards Sr(II).[17,18] Furthermore, its interlayer containing sodium cations are replaced by strontium along with a structural collapse, avoiding the trapped radioactive ions releasing to water again.

However, nanoscale of this adsorbent made it difficult for solid–liquid separation, especially under radioactive operating condition. Even if they were employed in column separation to avoid this issue, under-size and irregular particles lead to a surge of column pressure, and more importantly, inadequate strength and unsuitable mechanical properties rendered them unsuitable for industrial application. Therefore, a support material was needed to be introduced to overcome these shortcomings.

In recent years, many researchers focus on magnetic nanocomposite because of their rapid separation performance under external magnetic field. Decorating magnetic particle with specific extractant or ion exchange opened a new perspective for the separation of radionuclides, which combined the high adsorption capacity with advantage of magnetic separation.[19,20] Böhmer *et al.* functionalized magnetic silica particles with tetra-CMPO-calix[4]arenes to magnetically assisted removal of

[a]*School of Material Science and Engineering, Sun Yat-Sen University, Guangzhou 510275, China. E-mail: yirong280@163.com*

[b]*Institute of Nuclear and New Energy Technology (INET), Tsinghua University, Beijing 100084, China. E-mail: jingxia@tsinghua.edu.cn*

† Electronic supplementary information (ESI) available. See DOI: 10.1039/c9ra06148g

lanthanides and actinides,[21,22] which showed high adsorption efficiency towards Eu(III), Am(III), Ce(III). Yang *et al.* prepared magnetic Prussian blue/graphene oxide nanocomposites for the removal of radioactive cesium in water and its maximum adsorption capacity was up to 55.56 mg g^{-1}.[23] Song *et al.* fabricated a multi-shelled magnetic Fe_3O_4@MnO_x hollow composite and the adsorbent displayed considerable sorption capacities towards uranium (U(VI)) and europium (Eu(III)). According to their spectroscopic studies, U(VI) was proved to be adsorbed on the Mn^{III}–O–H site while Eu(III) shows higher affinity to the Mn^{IV}–O–H site.[24]

Therefore, from the perspective of practical application, the titanate fiber incorporated with magnetic particles will provide a promising technology for the removal of radioactive strontium. Until now, several studies have reported the fabrication strategy of magnetic titanate nanocomposites. Liu *et al.* utilized van der Waals interactions to synthesis a novel and facile acid-induced self-assembly process to tightly anchor Fe_3O_4 NPs onto the surfaces of titanate nanostructures.[25] Niu *et al.* prepared magnetic titanate nanotube through a co-precipitation process based on the exchange of protons with Fe^{2+}/Fe^{3+} ions, followed by functionalized with C_{18} groups for the efficient extraction of phthalate esters.[26] However, the Fe_3O_4 particle in their synthetic nanocomposite was naked, which were susceptible to air oxidation. Therefore, a protective layer was needed to be introduced onto the surface of Fe_3O_4 particle. Besides, to our knowledge, employing magnetic titanate fibers with core–shell structure for the removal of strontium (Sr(II)) have never been reported.

Herein, a new kind of core–shell structured magnetic microspheres decorated with titanate fibers was prepared for the removal of strontium, which was obtained from Fe_3O_4@SiO_2@TiO_2 under hydrothermal treatment at 160 °C in 10 M NaOH solution. The synthetic procedure was optimized and the morphology of the magnetic microspheres was detailed. In this process we found that the introduction of silica layer will benefit to the immobilization of titanate fibers. Adsorption kinetics and isotherms of magnetic microspheres towards Sr(II) were investigated through batch experiments. In addition, a possible adsorption mechanism was raised based on the variation of ions during adsorbing process and the X-ray photoelectron spectroscopy (XPS) analyses.

Experimental

Chemicals

Ferric chloride hexahydrate ($FeCl_3 \cdot 6H_2O$), anhydrous sodium acetate, ethylene glycol (EG), tetraethyl orthosilicate (TEOS) were purchased from Sigma-Aldrich. Tetrabutyl orthotitanate (TBOT) and hydroxypropyl cellulose (HPC) were supplied by J&K. All chemicals were analytical grade used without further purification. Deionized water was obtained from a Milli-Q water purification system.

Synthesis of Fe_3O_4@SiO_2@TiO_2 microspheres

The Fe_3O_4@SiO_2@TiO_2 microspheres were prepared as described in our previous work.[27] First, the magnetic core Fe_3O_4 was synthesized through a solvothermal method.[28] Briefly, 2.70 g of $FeCl_3 \cdot 6H_2O$ and 7.2 g of sodium acetate were dissolved in 100 mL ethylene glycol under magnetic stirring to obtain a homogeneous yellow solution. The mixed solution was then transferred into a Teflon-lined stainless-steel autoclave and heated at 200 °C for 8 h. Finally, the products was washed with ethanol and deionized water and dried in vacuum at 60 °C for 12 h.

To obtain Fe_3O_4@SiO_2@TiO_2 microspheres, the magnetite particles were coated with a thin layer of silica and titania *via* sol–gel approach, respectively. Typically, 0.5 g Fe_3O_4 particles was treated with 0.1 mol L^{-1} HCl aqueous solution by ultrasonication and washed with deionized water, followed by dispersion in a mixture of absolute ethanol (200 mL), deionized water (50 mL) and concentrated ammonia aqueous solution (2.5 mL, 28 wt%). Tetraethyl orthosilicate (TEOS, 0.5 mL) was added to the above solution drop by drop. After stirring at room temperature for 6 h, the Fe_3O_4@SiO_2 microspheres were separated by using a magnet, washed with ethanol and deionized water, and then mixed with deionized (3 mL), HPC (1.25 g) and absolute ethanol (400 mL). 5 mL of TBOT was added dropwise under vigorous mechanical stirring and the mixed solution was heated to 85 °C for 2.5 h. The product was washed with ethanol for three times and dried in vacuum at 60 °C for 8 h.

Preparation of Fe_3O_4@titanate nanofibers composite

Typically, Fe_3O_4@SiO_2@TiO_2 particles (0.2 g) was added to a solution of NaOH (25 mL, 10 M) followed by ultrasound for 15 min. The mixture was then placed into a Teflon-lined autoclave, sealed and hydrothermally treated at 160 °C for 48 h. The product was recovered with the help of magnet and washed with deionized water until a pH value was approximate 8. After an alcohol washing step, the sample was dried at 60 °C for 8 h in vacuum.

Ion-exchange experiments

The ion-exchange behavior of Sr(II) onto the magnetic titanate nanocomposites was studied by batch experiments. 10 mg of microspheres was added into 4 mL of $SrCl_2$ solution with a pH value of 6.5. The adsorption kinetic was investigated *via* altering contact time from 5 min to 240 min and the adsorption isotherm was determined by varying the initial strontium concentration between 0.05–0.5 g L^{-1}. After being shaking for specific contact time in 25 °C constant temperature bath oscillator, the solid phase was separated by using an NdFeB magnet and the aqueous solution was filtered with syringe-type filters. The concentration of strontium in the supernatant was analyzed by atomic absorption spectroscopy (AAS). The distribution coefficient (K_d) and adsorption capacity q_t were calculated by following equations:

$$K_d = \frac{C_0 - C_e}{C_0} \times \frac{V}{m} \quad (1)$$

$$q_t = \frac{(C_0 - C_t) \times V}{m} \quad (2)$$

where C_0, C_e and C_t represent aqueous strontium concentration at the initial time, at the equilibrium and at the time t, respectively; V is the volume of solution, and m is the mass of adsorbent.

Characterizations

X-ray diffraction (XRD) patterns of powder samples were recorded on a Bruker D8 Advance-X-ray diffractometer with monochromatized $Cu_{K\alpha}$ radiation ($\lambda = 1.5418$ Å). The size and morphology of magnetic microspheres was observed using ZEISS 1530 scanning electron microscope (SEM) and JEM 2011 transmission electron microscopes (TEM). Atomic Absorption Spectroscopy (AAS) was used to determine the concentration of metal ions. X-ray photoelectron spectroscopy (XPS) measurement was carried out on an Axis Ultra (Kratos Analytical Ltd) imaging photoelectron spectrometer using a monochromatized aluminum Kα anode, and the C 1s peak at 284.8 eV was taken as an internal standard.

Results and discussion

Characterization of materials

Fig. 1 shows the morphology of the Fe_3O_4, Fe_3O_4@SiO_2, Fe_3O_4@SiO_2@TiO_2 and Fe_3O_4@titanate. The magnetic core Fe_3O_4 particles (Fig. 1a) have a mean diameter of approximate 300 nm. After coating with silica *via* the typical Stöber method, an evident core–shell structure can be observed from Fig. 1b and the thickness of silica layer was about 20 nm. Since the titanate fibers can be obtained from the reaction between TiO_2 polymorphs and concentrated NaOH solution at lower hydrothermal temperatures,[29] a layer of titania was introduced as reagent to the Fe_3O_4@SiO_2 microspheres using sol–gel approach, resulting in an obvious thickness increase of shell layer (Fig. 1c). Finally, the resultant outer layer TiO_2 reacted with 10 M NaOH solution at hydrothermal under 160 °C. The obtained titanate fibers was deposited on the magnetic microspheres, forming Fe_3O_4/titanate nanofibers magnetic composite (Fig. 1d). In order to identify the pore structure and porosity of Fe_3O_4/titanate fibers, nitrogen adsorption–desorption characterization was conducted and the results were given in Fig. S1 and Table S1.† Due to the high proportion of magnetic core, the Fe_3O_4/titanate fibers showed a comparatively low specific surface area of 56.7 $m^2\ g^{-1}$ and pore volume of 0.2 $cm^3\ g^{-1}$. But its large average pore width contributed to mass transfer of adsorption process.

In synthetic process, the SiO_2 layer was destroyed because of its poor alkali resistance. However, element Si was still detected in the final composite through EDS study (Fig. S2†). In order to check its role in the deposition process of titanate fibers, a contrast trial was conducted without the silicon coating step, only a layer of TiO_2 was deposited onto the outside surface of Fe_3O_4 particle before hydrothermal treatment. Its image was shown in Fig. S3a,† which showed that the titanate nanofibers had not merged with magnetic precursor and were scattered independently. It is concluded that the SiO_2 layer contributed to the immobilization of titanate nanofibers.

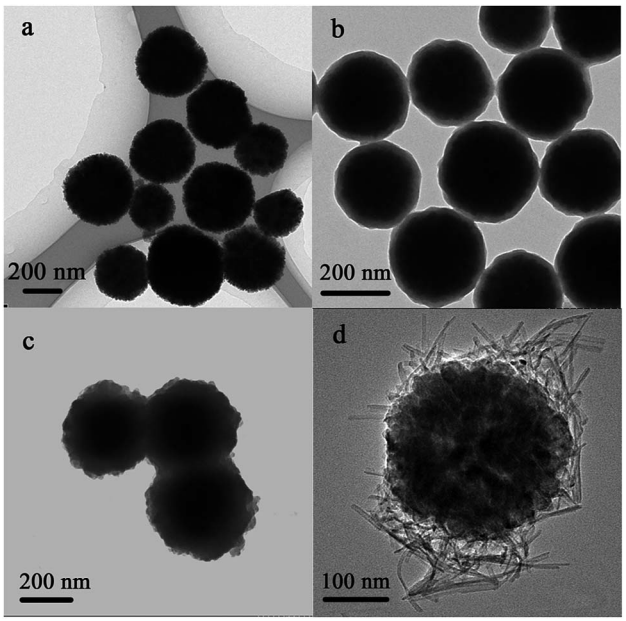

Fig. 1 TEM images of (a) Fe_3O_4 particles; (b) Fe_3O_4@SiO_2; (c) Fe_3O_4@SiO_2@TiO_2; (d) Fe_3O_4/titanate.

To further identify the structure of deposited titanate nanofiber, high resolution transmission electron microscopy (HRTEM) was utilized and its image was displayed in Fig. 2. It can be seen that the nanofiber possessed quite obvious layered structure, in which TiO_6-octahedra were the basic structure unit, each TiO_6 octahedron shared edges with other octahedra to form zigzag layer.[18] The exchangeable Na(I) ions were distributed in interlayers and can be substituted with other cations during ion exchange process.

The structure change during synthetic process was confirmed by XRD studies. Fig. 3a shows the XRD pattern of the Fe_3O_4@SiO_2@TiO_2 particles. All diffraction peaks only could be indexed to the magnetite phase of Fe_3O_4 (JCPDS 19-629), indicating that the SiO_2 and TiO_2 were both amorphous. However, after reacting with 10 M NaOH at 160 °C hydrothermal condition, the XRD pattern of final product, as shown in Fig. 3b, only matched well with the magnetite. No characteristic peaks of other materials were detected, which may be due to the low crystallinity of obtained titanate fibers. In order to improve this situation, the precursor, Fe_3O_4@SiO_2@TiO_2 particles, were calcinated at 500 °C for 2 h. The outer layer amorphous TiO_2 transformed to the anatase phase, which can be confirmed by the appearance of new peaks in Fig. 3c. All of them can be indexed to the anatase phase of TiO_2 (JCPDS 21-1272).[30] But all the diffraction peaks of anatase disappeared after treated with 10 M NaOH in a Teflon-lined autoclave at 160 °C. This result implied that enhancing the crystallinity of reagent TiO_2 did not contribute to the improvement of crystallinity in final product.

The surface morphology evolution after calcination treatment of precursor was revealed by SEM. The micrograph of the Fe_3O_4/titanate obtained from uncalcined Fe_3O_4@SiO_2@TiO_2 particles was provided in Fig. 4a. It can be seen that plenty of titanate fibers covered the surface of final product. On the other

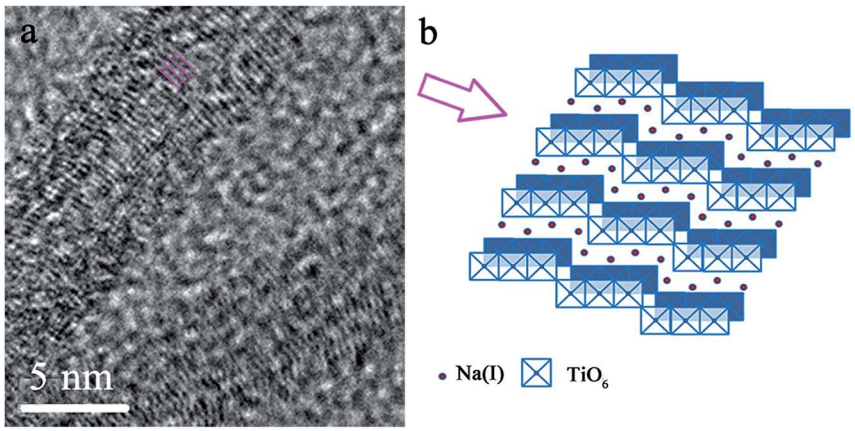

Fig. 2 HRTEM image of Fe_3O_4/titanate (a) and the schematic structure of titanate nanofibers (b).

hand, the Fe_3O_4/titanate prepared from Fe_3O_4@SiO_2@TiO_2 particles after calcination at 500 °C were nanosheets aggregates of titanate, as is evident from the image shown in Fig. 4b. The composition of Fe_3O_4/titanate nanofibers was verified by EDS

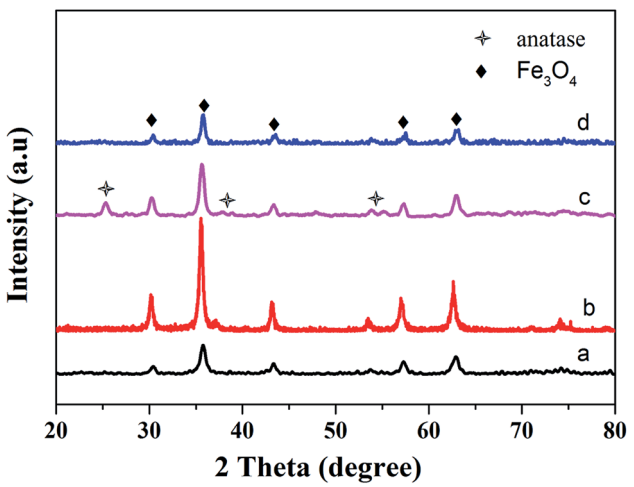

Fig. 3 XRD patterns of (a) Fe_3O_4@SiO_2@TiO_2 particles; (b) Fe_3O_4/titanate; (c) Fe_3O_4@SiO_2@TiO_2 after calcination at 500 °C for 2 h; (d) Fe_3O_4/titanate obtained from calcined Fe_3O_4@SiO_2@TiO_2 particles at 500 °C for 2 h.

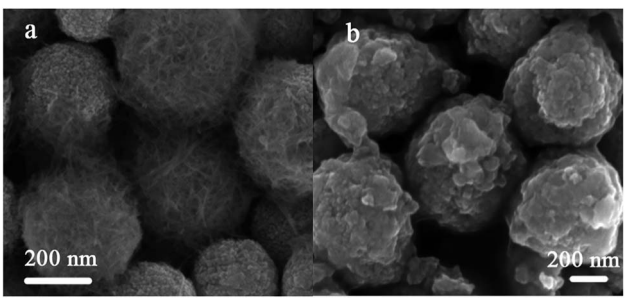

Fig. 4 SEM images of Fe_3O_4/titanate nanofibers (a) and Fe_3O_4/titanate nanosheets (b).

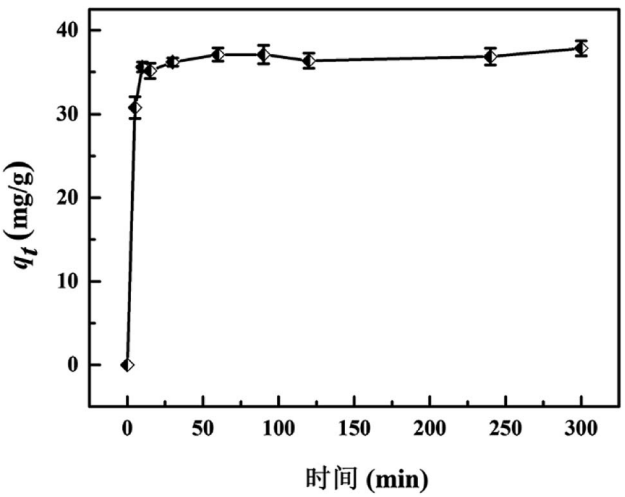

Fig. 5 Effect of contact time on the removal of Sr(II) by Fe_3O_4/titanate nanofibers.

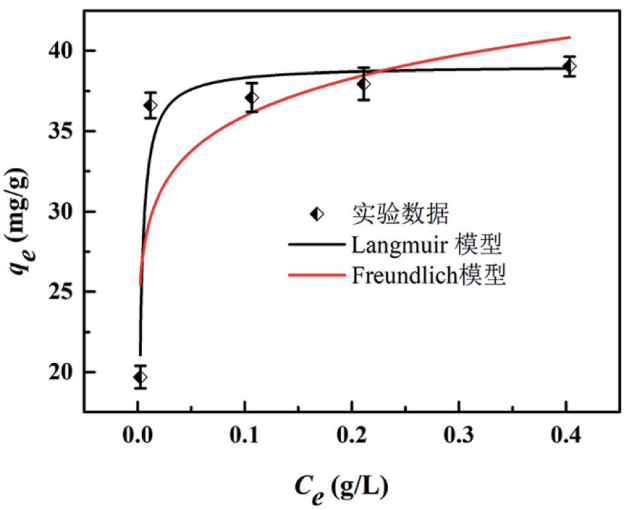

Fig. 6 Adsorption isotherms of Sr(II) on Fe_3O_4/titanate fibers.

Table 1 Comparison of Sr(II) adsorption performance between different magnetic adsorbents

Adsorbent	Equilibrium time	Adsorption capacity (mg g^{-1})	Ref.
Multiwall carbon nanotube/iron oxide magnetic	40 min	9.18	32
Graphene oxide-magnetite	5 h	14.1	33
Magnetic polyaniline/graphene oxide	12 h	37.17	34
Magnetic Fe_3O_4 particles modified sawdust	30 min	12.59	35
Bis(trimethoxysilypropyl) functionalized magnetic particles	90 min	3.15	36
Magnetic clinoptilolite/$CoFe_2O_4$ composites	1200 min	20.58	37
Synthesized magnetic chitosan beads	6 h	11.58	38
Magnetic Sr(II)-imprinted polymer	120 min	54.49	39
Alginat/Fe_3O_4 composite	6 h	12.5	40
Magnetic microspheres impregated with crown ether	10 h	9.05	41
Magnetic titanate nanofibers	30 min	37.1	This work

(Fig. S2 and Table S2†), which exhibited the existence of Na and Ti with a molar radio close to 2 : 3. This was consistent with $Na_2Ti_3O_7$.

Adsorption behavior study

Adsorption kinetics. It is necessary to investigate the adsorption kinetic in the process of strontium adsorption, which is of great significance for the practical use of adsorption materials. Fig. 5 shows the adsorption rate of Fe_3O_4/titanate fibers for Sr(II) with initial concentration of 200 ppm at pH = 6.5. The adsorption process was very fast and the equilibrium was established within 30 min. The rapid uptake rate may result from its large specific surface area and fiber structure.

Adsorption isotherm. To investigate the adsorption capacities, the adsorption isotherm of Fe_3O_4/titanate fibers toward Sr(II) was obtained by varying the initial concentration of Sr(II) from 0.05 to 0.5 g L^{-1}. Adsorption capacity q_e (mg g^{-1}) *versus* concentration of Sr(II) at equilibrium C_e (g L^{-1}) was plotted in Fig. 6. It can be seen that the growth trend of q_e was analogous to that in the kinetics experiments. The adsorption capacity undergoes a rapid increase when the initial concentration of Sr(II) is less than 0.1 g L^{-1}, followed by a sluggish growth pace with the increasing of Sr(II) concentration. In order to describe the adsorption of Sr(II)-adsorption by Fe_3O_4/titanate fibers magnetic composite, Langmuir and Freundlich adsorption isotherm model were employed for the adsorption analysis to fit with the experiment data, which was used to describe single-layer adsorption with all free binding sites and multi-layer adsorption with several kinds of adsorption sites, respectively. These two models can be expressed in the following form separately:[31]

$$q_e = q_{max}\frac{KC_e}{1 + KC_e} \quad (3)$$

$$q_e = K_F C_e^{1/n} \quad (4)$$

where C_e (mg L^{-1}) is the equilibrium concentration of strontium, q_e (mg g^{-1}) is the amount of Sr(II) adsorbed per unit weight of the adsorbent at equilibrium, q_{max} (mg g^{-1}) represents the monolayer maximum adsorption capacity. K is the equilibrium constant related to the enthalpy of sorption in Langmuir isotherm model. K_F and n are the Freundlich constants relative to the multilayer adsorption capacity and adsorption intensity, respectively.

As shown in Fig. 6, the Langmuir adsorption isotherm model fit well with experiment data better, suggesting that the adsorbent surface was heterogeneous. The Langmuir isotherm constants and their correction coefficients were listed in Table S3† and the maximum adsorption capacity was calculated to be 39.08 mg g^{-1}.

Comparison of various magnetic adsorbents

A comparison between Fe_3O_4/titanate fibers and some other reported magnetic composites for Sr(II) adsorption was conducted and the results were presented in Table 1.[32–41] It can be seen that the magnetic titanate nanofibers exhibits excellent adsorption ability among magnetic composite used for Sr(II) removal. Although some magnetic adsorbents, such as magnetic polyaniline/graphene oxide, magnetic Sr(II)-imprinted polymer, shows high adsorption capacity towards Sr(II) as well,

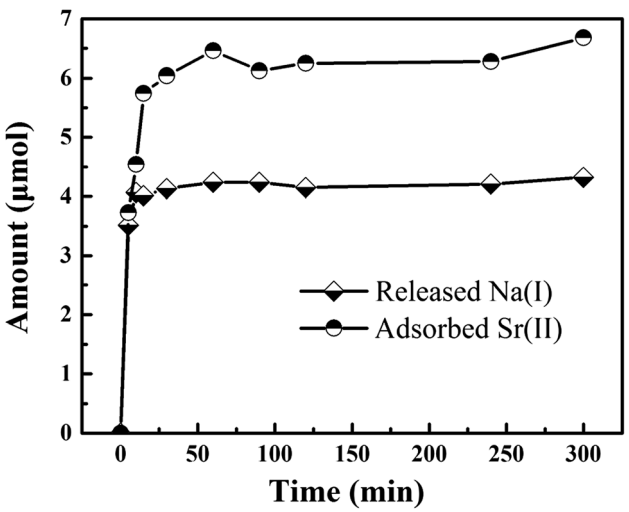

Fig. 7 The effect of contact time on the variation of Na(I) and Sr(II) during adsorption process.

the time for establishing adsorption equilibrium is more than 2 h. By contrast, the magnetic titanate nanofibers is endowed with rapid Sr(II) uptake rate and the adsorption equilibrium can be reach within 30 min.

Elution and reusability

^{90}Sr is a common β radioactive source. Regeneration of adsorbed Sr(II) will yield some economical benefit. Moreover, it can contribute to reduction and degradation of radioactive waste. Therefore, it necessary to investigate the elution of adsorbed Sr(II) by using various eluent and the results is shown in Table S4.† It could be clearly observed that the captured Sr(II) can be eluted by using 5 wt% of EDTA(Na) and desorption rate is up to 92.2%. However, when the composite is reused for Sr(II) removal, the adsorption ability experienced a significant decline. Similar phenomenon can be found in many reported synthetic ion exchangers for Sr(II) uptake, resulted from the collapses of interlayered structure.[11,14,42] As for titanate nanofibers, when part of the Na(I) ions is replaced by Sr(II), a significant reduction of the interlayer spacing (d_{100}) can be observed and the (003) planes is found to be substantial deformation because of the strong interaction between the (003) planes and the Sr(II) ions.[18] Owing to the strong affinity between the Sr(II) ions and the negatively charged layers in titanate nanofiber, the magnetic composite was endowed with high selectively toward Sr(II) and it was difficult for the absorbed Sr(II) to release into the environment again.

Adsorption mechanism

Based on the previous study, the adsorption of titanate toward ions was the process of Na(I) replacement by Sr(II), which existed in interlayers of adsorbent. Therefore, we supposed the Sr(II) are entirely exchanged with Na(I) during the adsorption of Fe_3O_4/titanate fibers towards Sr(II). The variation of ions with the increasing of contact time, including released Na(I) and adsorbed Sr(II), can be monitored. The changing amount *versus* time were plotted in Fig. 7. It is noted that sodium ions appear in the solution after adsorption and the concentration increases with the increase of adsorbed strontium ions. However, the radio between the molar amount of released Na(I) and the amount of adsorbed Sr(II) was calculated to be about 1.7, not up to 2, indicating other components were likely to be involved in the Sr(II) adsorption.

In order to further confirm the adsorption mechanism, the XPS of the samples before (MT3) and after Sr(II) adsorption (MT3-Sr) were measured. To further understand the electronic states of the elements and investigate the interaction between the functional groups of Fe_3O_4/titanate fibers and Sr(II), high resolution spectra of Na 1s, Sr 3d, Fe 2p, Ti 2p and O 1s were recorded and the results were presented in Fig. 8. Direct

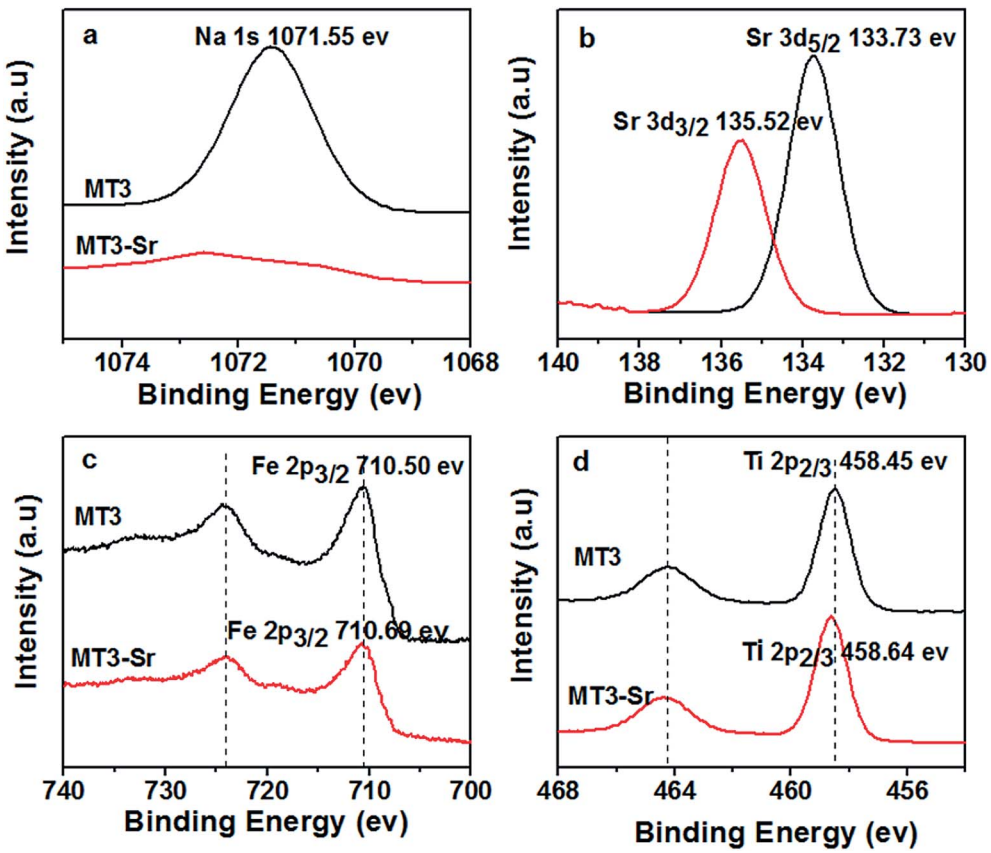

Fig. 8 XPS high resolution spectra of (a) Na 1s, (b) Sr 3d (c) Fe 2p and (d) Ti 2p before and after Sr(II) adsorption; Sr 3d spectrum of the Sr(II)-adsorbed sample.

evidence for an ion exchange process between Sr(II) and Na(I) ions which existed in the interlayers of the titanate were found in Fig. 8a and b. After Sr^{2+} adsorption, the peak at 1071.55 eV (Fig. 8a) assigned to the Na 1s peak disappeared, indicating that Na(I) ions were almost completely exchanged. Meanwhile, a double characteristic peak of Sr(II) 3d at 133.73 and 135.52 eV (Fig. 8b) appear in the spectrum of adsorbed sample, which were contribute to the Sr $3d_{5/2}$ and Sr $3d_{3/2}$, respectively. In the Fe 2p spectrum, a slight shift of Fe 2p peaks at 710.50 and 724.40 eV were observed, revealing that Fe_3O_4 was involved in the adsorption of Sr(II), which accounted for the phenomenon that the radio between the molar amount of released Na(I) and the amount of adsorbed Sr(II) was less than 2. Besides, the Ti 2p peaks (Fig. 8d) at 458.45 and 464.25 eV are shifted to higher binding energies on account of the interaction between TiO_6 octahedron and Sr(II). From the O 1s higher-resolution deconvolution spectra of Fig. S4,† three different peaks centered at 529.97, 531.30 and 532.66 eV were observed. The peak at 529.97 eV was attributed to O 1s of TiO_6 or FeO_6 octahedra and was shifted to a higher binding energy after Sr(II) adsorption (Fig. S5†).

Conclusions

In this paper, a novel core–shell structured magnetic nanocomposite sorbent Fe_3O_4@titanate fiber was prepared through hydrothermal and sol–gel process. The composite showed high exchangeable capacity towards strontium due to the introduction of sodium titanate. Batch experiments showed that the exchange balance can be established within 30 min and adsorption isotherm fits well with the Langmuir isotherm model. The maximum exchange capacity was approximately 37.1 mg g^{-1}. Through monitoring the variation of ions with the increasing of contact time and employing XPS analysis, a possible adsorption mechanism was raised that naked Fe_3O_4 particle and the titanate fiber contribute to the removal of Sr(II). This novel magnetic composite shows great potential for the strontium removal from wastewater.

Conflicts of interest

There are no conflicts of interest to declare.

Acknowledgements

The study was supported by the National Natural Science Foundation of China under Project 51425403 and 51473087.

References

1 R. Yi, G. Ye, F. C. Wu, M. F. Wen, X. G. Feng and J. Chen, *RSC Adv.*, 2014, **4**, 37600–37608.
2 M. Ishizaki, S. Akiba, A. Ohtani, Y. Hoshi, K. Ono, M. Matsuba, T. Togashi, K. Kananizuka, M. Sakamoto, A. Takahashi, T. Kawamoto, H. Tanaka, M. Watanabe, M. Arisaka, T. Nankawa and M. Kurihara, *Dalton Trans.*, 2013, **42**, 16049–16055.
3 E. Wieland, J. Tits, D. Kunz and R. Dähn, *Environ. Sci. Technol.*, 2008, **42**, 403–409.
4 S. Langley, A. G. Gault, A. Ibrahim, Y. Takahashi, R. Renaud, D. Fortin, I. D. Clark and F. G. Ferris, *Environ. Sci. Technol.*, 2009, **43**, 1008–1014.
5 H. Liu and J. Wang, *J. Hazard. Mater.*, 2013, **261**, 307–315.
6 F. Jia, Y. Yin and J. Wang, *Prog. Nucl. Energy*, 2018, **103**, 20–27.
7 K. P. Lee, T. C. Arnot and D. Mattia, *J. Membr. Sci.*, 2011, **370**, 1–22.
8 S. Lee, Y. Kim, J. Park, H. K. Shon and S. Hong, *J. Membr. Sci.*, 2018, **556**, 238–247.
9 T. J. Stockmann, Y. Lu, J. Zhang, H. H. Girault and Z. Ding, *Chem.–Eur. J.*, 2011, **17**, 13206–13216.
10 S. Sarina, A. Bo, D. Liu, H. Liu, D. Yang, C. Zhou, N. Maes, S. Komarneni and H. Zhu, *Chem. Mater.*, 2014, **26**, 4788–4795.
11 W. J. Paulus, S. Komarneni and R. Roy, *Nature*, 1992, **357**, 571–573.
12 T. Kodama, Y. Harada, M. Ueda, K. Shimizu, K. Shuto and S. Komarneni, *Langmuir*, 2001, **17**, 4881–4886.
13 R. Yavari, S. J. Ahmadi, Y. D. Huang, A. R. Khanchi, G. Bagheri and J. M. He, *Talanta*, 2009, **77**, 1179–1184.
14 D. Yang, Z. Zheng, H. Liu, H. Zhu, X. Ke, Y. Xu, D. Wu and Y. Sun, *J. Phys. Chem. C*, 2008, **112**, 16275–16280.
15 D. Yang, H. Liu, L. Liu, S. Sarina, Z. Zheng and H. Zhu, *Nanoscale*, **5**, 11011–11018.
16 D. Yang, Z. Zheng, Y. Yuan, H. Liu, E. R. Waclawik, X. Ke, M. Xie and H. Zhu, *Phys. Chem. Chem. Phys.*, 2010, **12**, 1271–1277.
17 D. J. Yang, Z. F. Zheng, H. Y. Zhu, H. W. Liu and X. P. Gao, *Adv. Mater.*, 2008, **20**, 2777–2781.
18 D. Yang, H. Liu, Z. Zheng, S. Sarina and H. Zhu, *Nanoscale*, 2013, **5**, 2232–2242.
19 M. Liu, C. Chen, T. Wen and X. Wang, *Dalton Trans.*, 2014, **43**, 7050–7056.
20 L. Tan, X. Zhang, Q. Liu, J. Wang, Y. Sun, X. Jing, J. Liu, D. Song and L. Liu, *Dalton Trans.*, 2015, **44**, 6909–6917.
21 V. Böhmer, J. F. Dozol, C. Gruttner, K. Liger, S. E. Matthews, S. Rudershausen, M. Saadioui and P. S. Wang, *Org. Biomol. Chem.*, 2004, **2**, 2327–2334.
22 S. E. Matthews, P. Parzuchowski, A. Garcia-Carrera, C. Gruttner, J. F. Dozol and V. Böhmer, *Chem. Commun.*, 2001, 417–418.
23 H. Yang, L. Sun, J. Zhai, H. Li, Y. Zhao and H. Yu, *J. Mater. Chem. A*, 2014, **2**, 326–332.
24 S. Song, S. Zhang, S. Huang, R. Zhang, L. Yin, Y. Hu, T. Wen, L. Zhuang, B. Hu and X. Wang, *Chem. Eng. J.*, 2019, **355**, 697–709.
25 F. Liu, Y. Jin, H. Liao, L. Cai, M. Tong and Y. Hou, *J. Mater. Chem. A*, 2013, **1**, 805–813.
26 H. Niu, S. Zhang, X. Zhang and Y. Cai, *ACS Appl. Mater. Interfaces*, 2010, **2**, 1157–1163.
27 R. Yi, G. Ye, F. Wu, M. Wen, X. Feng and J. Chen, *RSC Adv.*, 2014, **4**, 37600–37608.
28 Y. Deng, D. Qi, C. Deng, X. Zhang and D. Zhao, *J. Am. Chem. Soc.*, 2007, **130**, 28–29.

29 H. Y. Zhu, Y. Lan, X. P. Gao, S. P. Ringer, Z. F. Zheng, D. Y. Song and J. C. Zhao, *J. Am. Chem. Soc.*, 2005, **127**, 6730–6736.
30 M. Ye, Q. Zhang, Y. Hu, J. Ge, Z. Lu, L. He, Z. Chen and Y. Yin, *Chem.–Eur. J.*, 2010, **16**, 6243–6250.
31 C. Cao, F. Wei, J. Qu and W. Song, *Chem.–Eur. J.*, 2013, **19**, 1558–1562.
32 C. Chen, J. Hu, D. Shao, J. Li and X. Wang, *J. Hazard. Mater.*, 2009, **164**, 923–928.
33 A. Tayyebi, M. Outokesh, S. Moradi and A. Doram, *Appl. Surf. Sci.*, 2015, **353**, 350–362.
34 B. Hu, M. Qiu, Q. Hu, Y. Sun, G. Sheng, J. Hu and J. Ma, *ACS Sustainable Chem. Eng.*, 2017, **5**, 6924–6931.
35 Z. Cheng, Z. Gao, W. Ma, Q. Sun, B. Wang and X. Wang, *Chem. Eng. J.*, 2012, **209**, 451–457.
36 X. Ye, T. Liu, Q. Li, H. Liu and Z. Wu, *Colloids Surf., A*, 2008, **330**, 21–27.
37 Y. Huang, W. Wang, Q. Feng and F. Dong, *J. Saudi Chem. Soc.*, 2017, **21**, 58–66.
38 Y. Chen and J. Wang, *Nucl. Eng. Des.*, 2012, **242**, 445–451.
39 L. Yan, C. Rui, D. Yuan, Z. Liu, M. Meng, W. Yun, J. Han, X. Meng, F. Liu and Z. Hu, *Colloid Polym. Sci.*, 2015, **293**, 109–123.
40 H. Hong, H. S. Jeong, B. Kim, J. Hong, I. Park, T. Ryu, K. Chung, H. Kim and J. Ryu, *Chemosphere*, 2016, **165**, 231–238.
41 R. Yi, G. Ye, F. Wu, D. Lv and J. Chen, *J. Radioanal. Nucl. Chem.*, 2016, **308**, 599–608.
42 D. V. Marinin and G. N. Brown, *Waste Manag.*, 2000, **20**, 545–553.